Science Advances
AAAS

Supplementary Materials for

Brain injury accelerates the onset of a reversible age-related microglial phenotype associated with inflammatory neurodegeneration

Rodney M. Ritzel *et al.*

Corresponding author: Rodney M. Ritzel, rodney.m.ritzel@uth.tmc.edu;
David J. Loane, loanedj@tcd.ie; Junfang Wu, junfang.wu@som.umaryland.edu

Sci. Adv. **9**, eadd1101 (2023)
DOI: 10.1126/sciadv.add1101

This PDF file includes:

Supplemental Figure 1

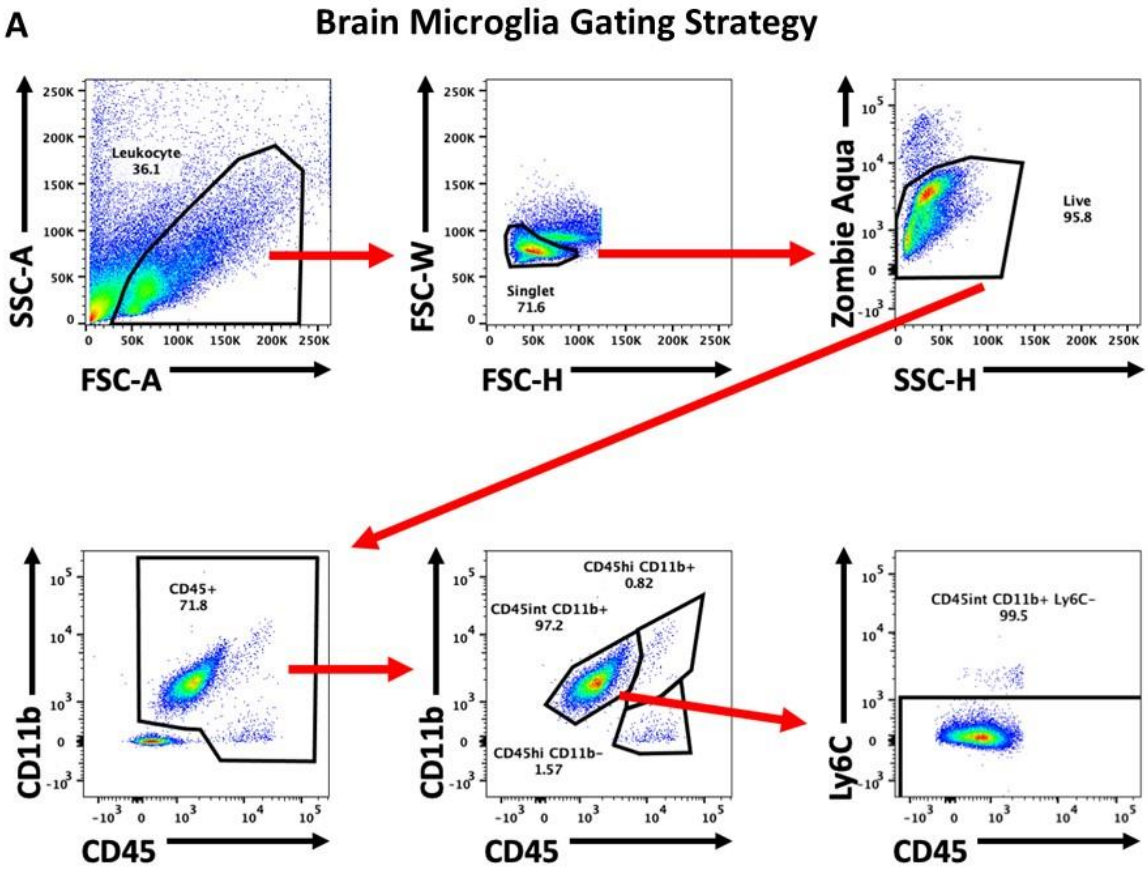

Fig. S1. Flow cytometry identification of microglia.
(A) Microglial cells in the brain were identified using the following gating strategy: leukocytes were first identified using a light scatter reference, then singlet gating, viable live cells, CD45 expression, $CD45^{int}CD11b^{+}$ expression, and finally, Ly6C-negative expression. Abbreviations: FSC forward scatter, hi high, int intermediated, SSC side scatter.

Supplemental Figure 2

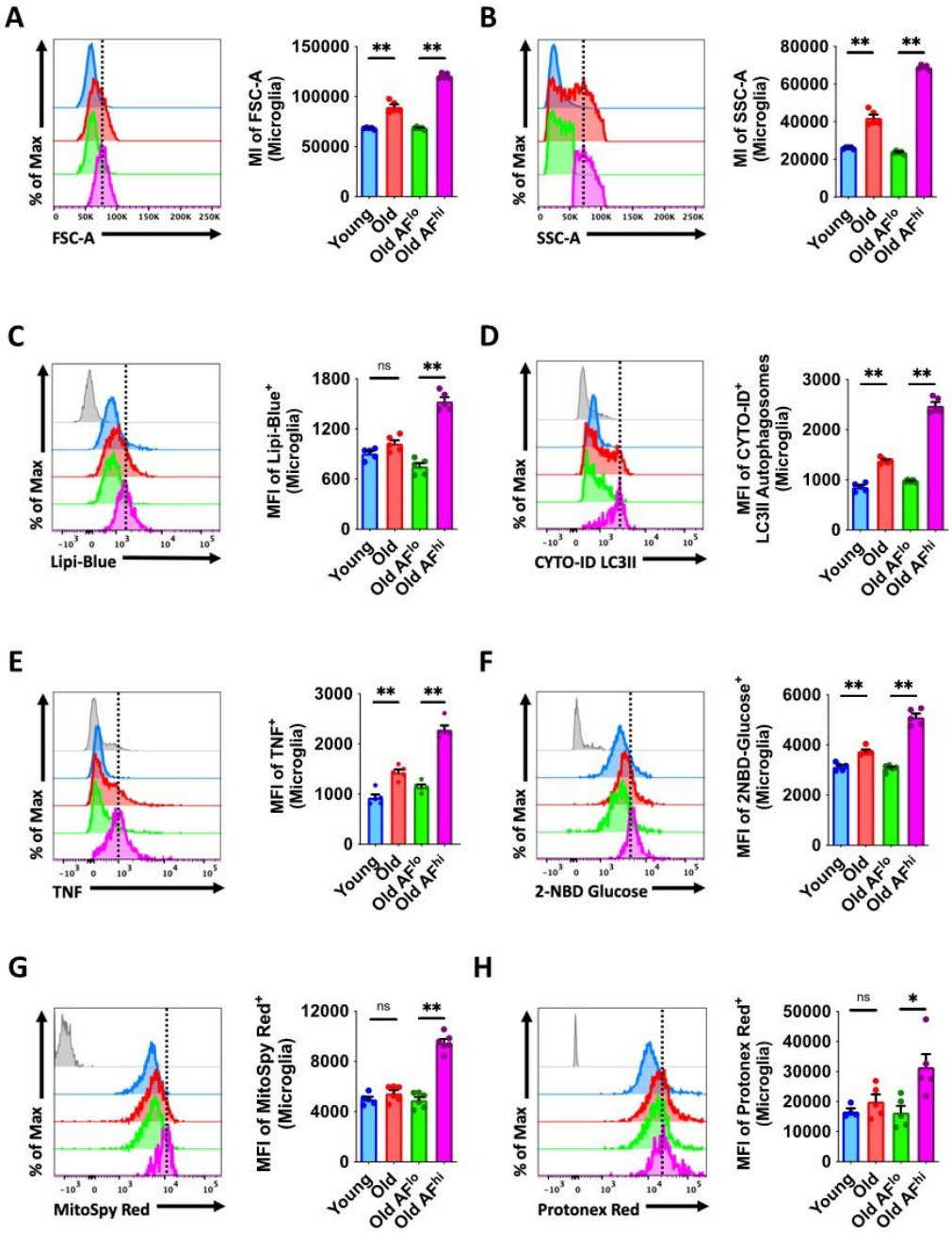

Fig. S2. Functional evaluation of AF microglia from aged mice.
Significant changes in cellular function of old AF^{hi} versus old AF^{lo} microglia subsets largely account for the age-related differences found in the general cell population. Representative histograms show that Old AF^{hi} microglia exhibit increases in **(A)** cell volume, **(B)** cell granularity, **(C**) lipid content, **(D)** autophagosome formation, **(E)** TNF production, **(F)** glucose uptake, **(G)** mitochondrial membrane potential, and **(H)** cytosolic acidosis. N=5/group. Abbreviations: AF autofluorescent, FSC forward scatter, hi high, lo low, Max maximum, MFI mean fluorescence intensity, ns not significant, SSC side scatter. Non-parametric data were analyzed using Mann-Whitney test (**p<0.01, ***p<0.001 and ****p<0.0001).

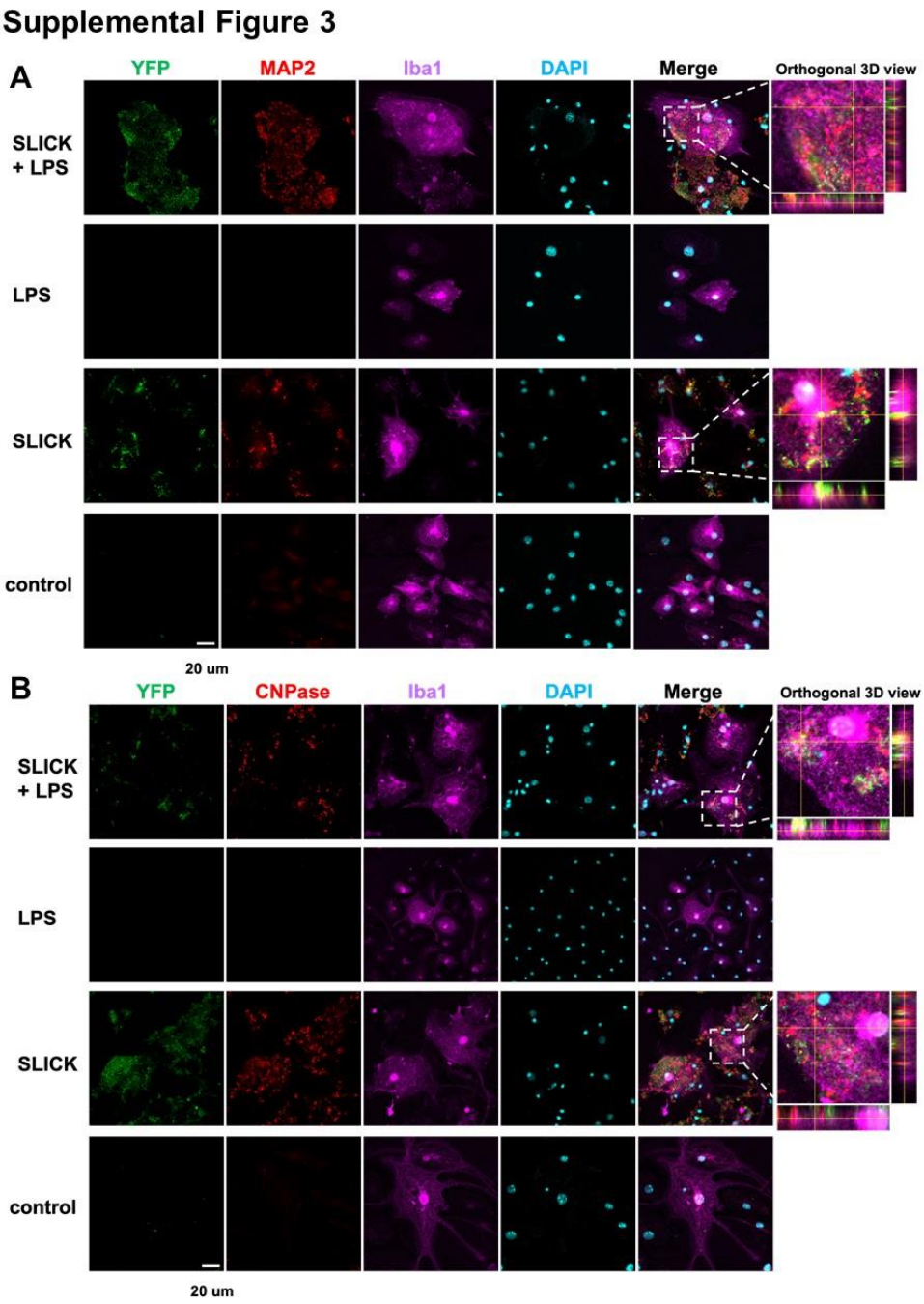

Fig. S3. Cell culture validation of *ex vivo* neuronal engulfment assay.
Phagocytosis of SLICK-YFP neurons and myelin by neonatal microglia was demonstrated *in vitro* with and without lipopolysaccharide stimulation (100 ng/ml, 2h) via immunocytochemistry. Two independent experiments were performed to demonstrate the specificity of MAP2 (**A**, in red) and myelin CNPase (**B**, in red) monoclonal antibodies. In the absence of SLICK-YFP neurons (in green), MAP2 neuronal antigen and myelin CNPase antigens were not detected. Abbreviations: LPS lipopolysaccharide, YFP yellow fluorescent protein, MAP2 Microtubule Associated Protein 2, 3D three-dimensional, DAPI 4′,6-diamidino-2-phenylindole, Iba1 ionized calcium-binding adapter molecule 1, SLICK single-neuron labeling with inducible Cre-mediated knock-out.

Supplemental Figure 4

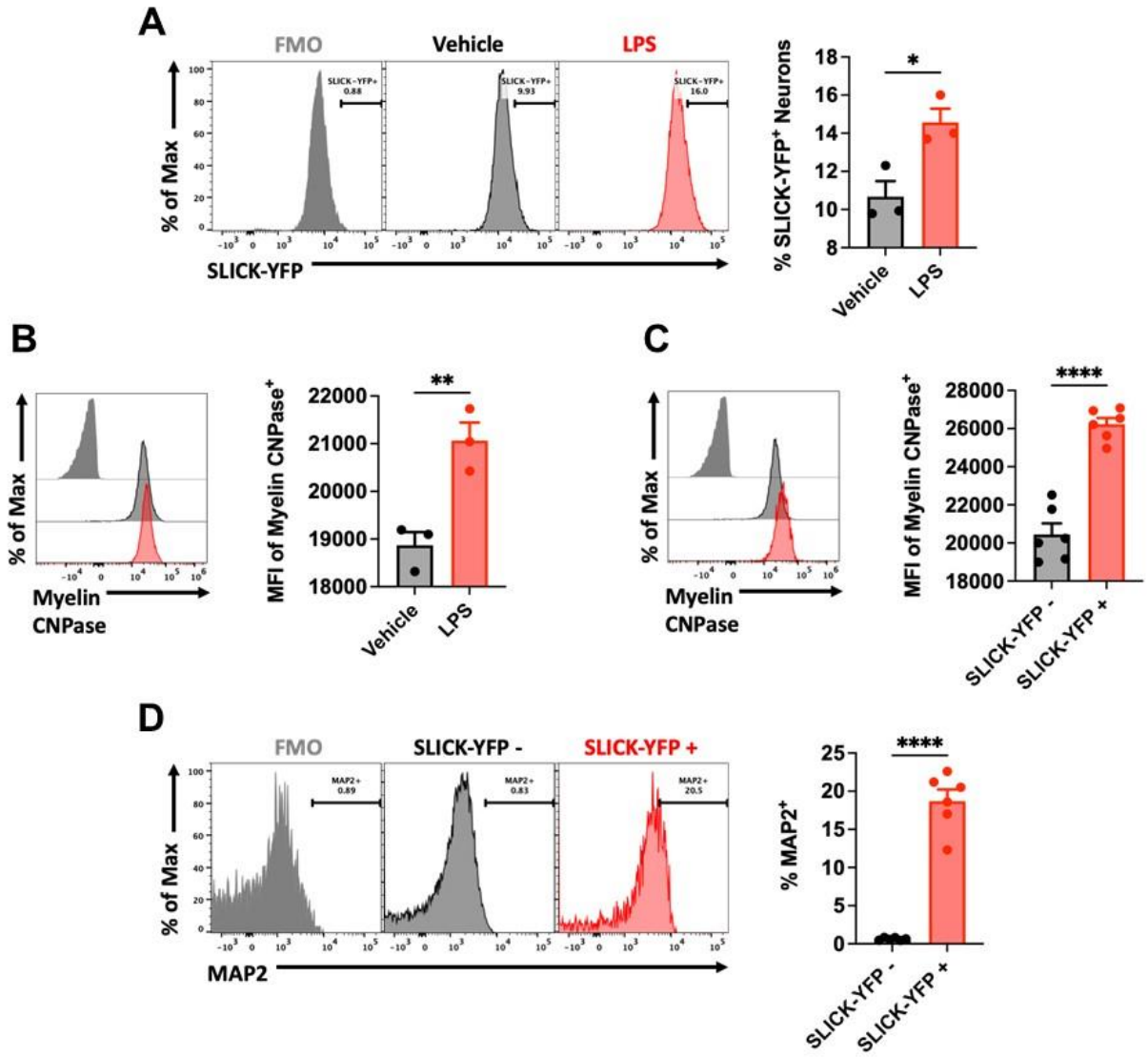

Fig. S4. Flow cytometry validation of *ex vivo* neuronal engulfment assay.
Phagocytosis of SLICK-YFP neurons and myelin by neonatal microglia was demonstrated *in vitro* with and without lipopolysaccharide (LPS) stimulation (100 ng/ml, 2h) via flow cytometry. Vehicle and LPS groups were incubated with feeder neurons. LPS stimulation induced microglial phagocytosis of SLICK-YFP neurons (**A**) and intracellular accumulation of myelin CNPase antigen (**B**). Microglia that engulfed myelinated SLICK-YFP cortical neurons had significantly higher levels of intracellular myelin CNPase than non-phagocytic microglia (**C**). Neuronal-derived MAP2 was exclusively detected in phagocytic (i.e., SLICK-YFP-positive) microglia (**D**). Abbreviations: FMO fluorescence minus one, LPS lipopolysaccharide, Max maximum, YFP yellow fluorescent protein, MFI mean fluorescence intensity, MAP2 Microtubule Associated Protein 2. N=3-6/group. Data were analyzed by Student's t-test (*p<0.05, **p<0.01, and ****p<0.0001).

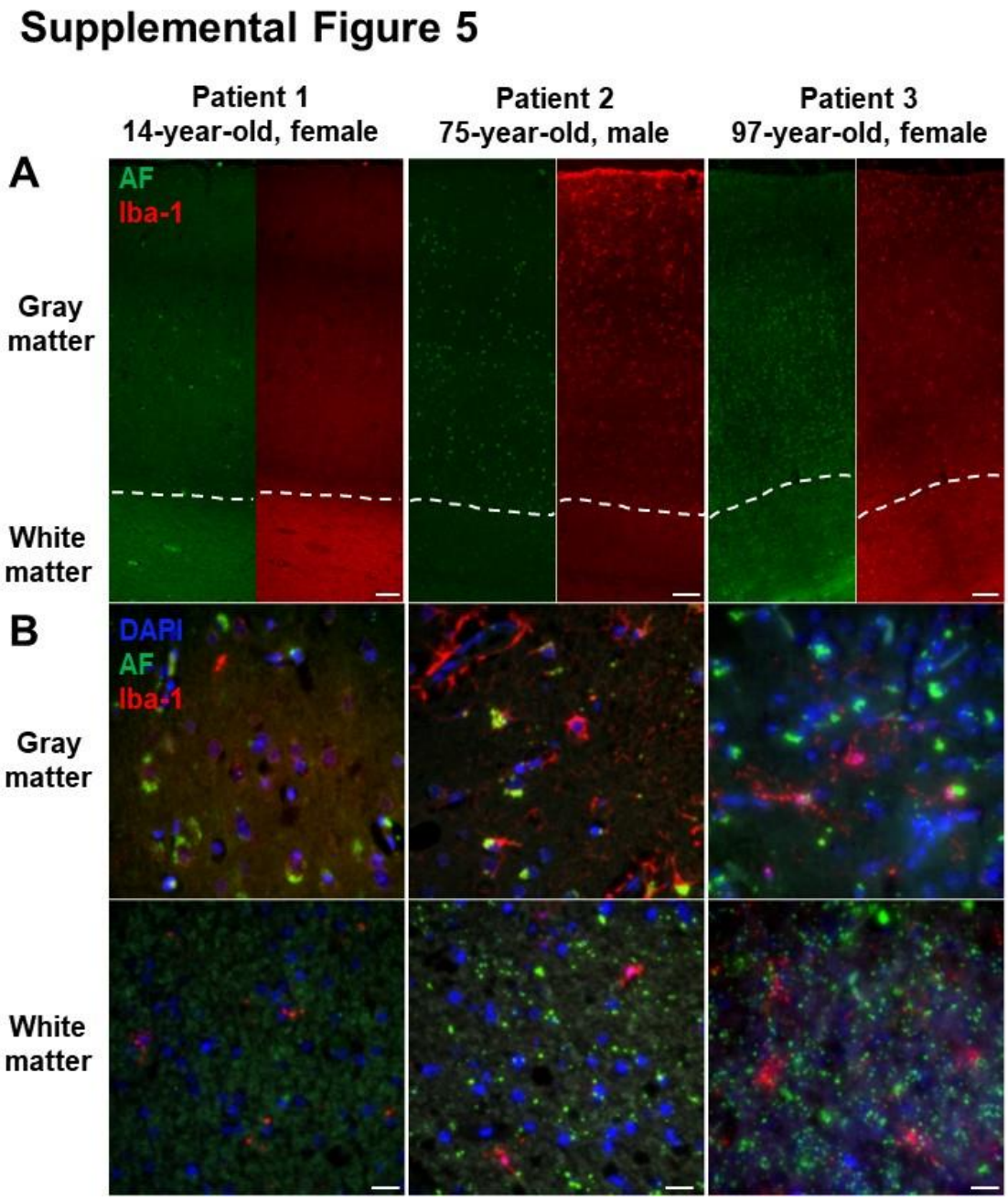

Fig. S5. Evidence and distribution of autofluorescent microglia in cortical sections of post-mortem human brain tissue.

Immunohistochemistry was performed on human control brains in which no neuropathology was diagnosed before or after autopsy. Microglial autofluorescence in gray and white matter is shown in the somatosensory and visual cortex of young adult (Patient 1, 14-year-old), aged 1 (Patient 2, 75-year-old), and aged 2 (Patient 3, 97-year-old). AF puncta (in green, empty FITC channel) can be seen inside Iba-1-positive microglia/macrophages (in red) countered stained with DAPI (in blue). AF microglia are more noticeable in the gray versus white matter regions of the cortex at all ages. Scale bars = 100 μm (**A**) and 20 μm (**B**). Abbreviations: AF autofluorescence, Iba-1 ionized calcium-binding adapter molecule 1, DAPI 4′,6-diamidino-2-phenylindole.

Supplemental Figure 6

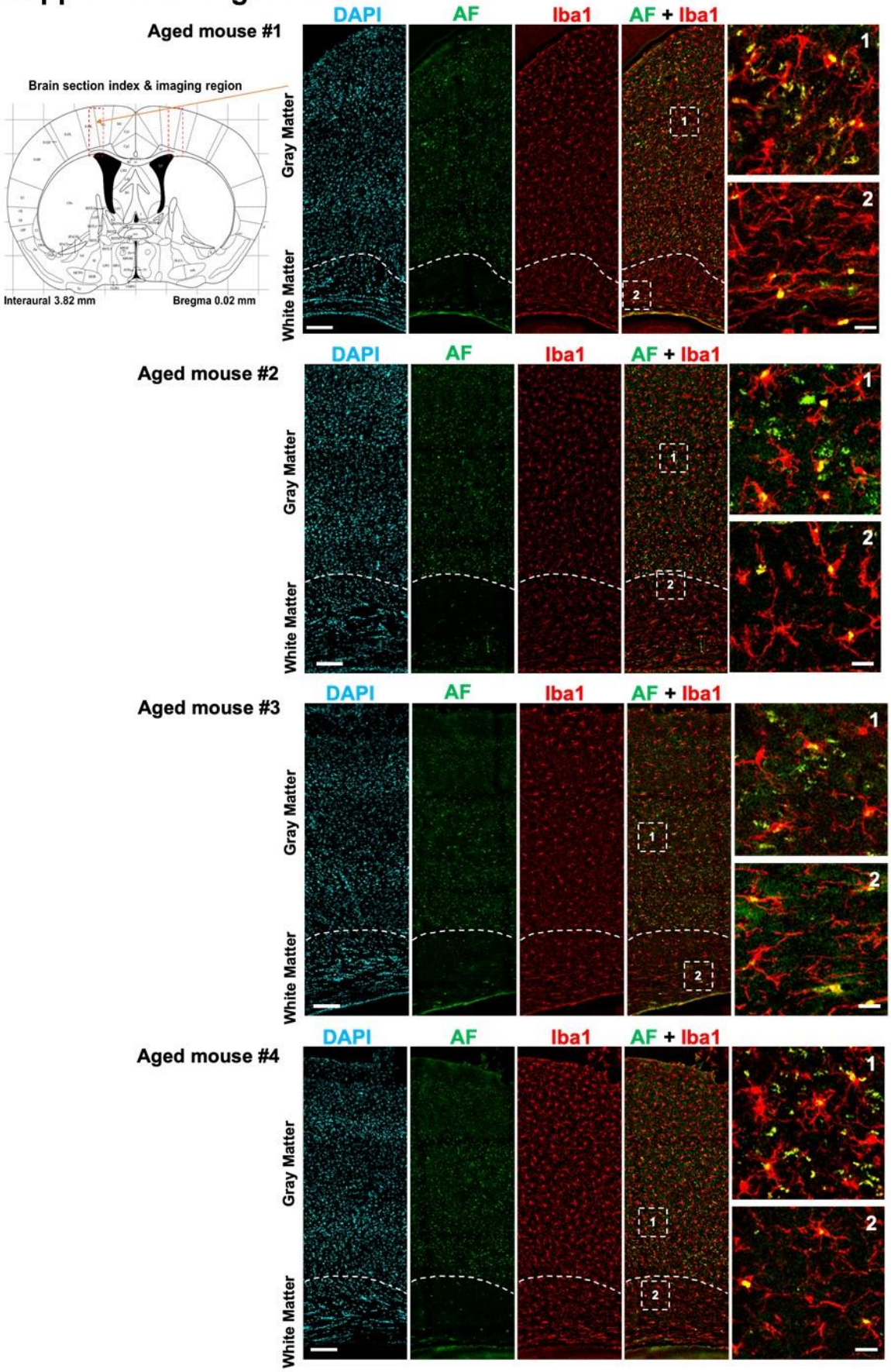

Fig. S6. Distribution of autofluorescent microglia in the aged murine cortex.
Immunohistochemistry was performed on coronal brain sections of normal aged (18-month-old) male mice. Microglial autofluorescence in gray and white matter is shown in the indicated cortex according to the anatomical diagram (top left). Images from four individual mice are shown. AF puncta (in green, empty FITC channel) can be seen inside Iba1-positive microglia/macrophages (in red) countered stained with DAPI (in blue). Upon higher magnification, AF microglia are especially apparent in the gray (labeled box 1) versus white matter (labeled box 2) regions within the same cortical section. Scale bars =100 μm (left panels) and 20 μm (right panels). Abbreviations: AF autofluorescence, Iba1 ionized calcium-binding adapter molecule 1, DAPI 4′,6-diamidino-2-phenylindole.

Supplemental Figure 7

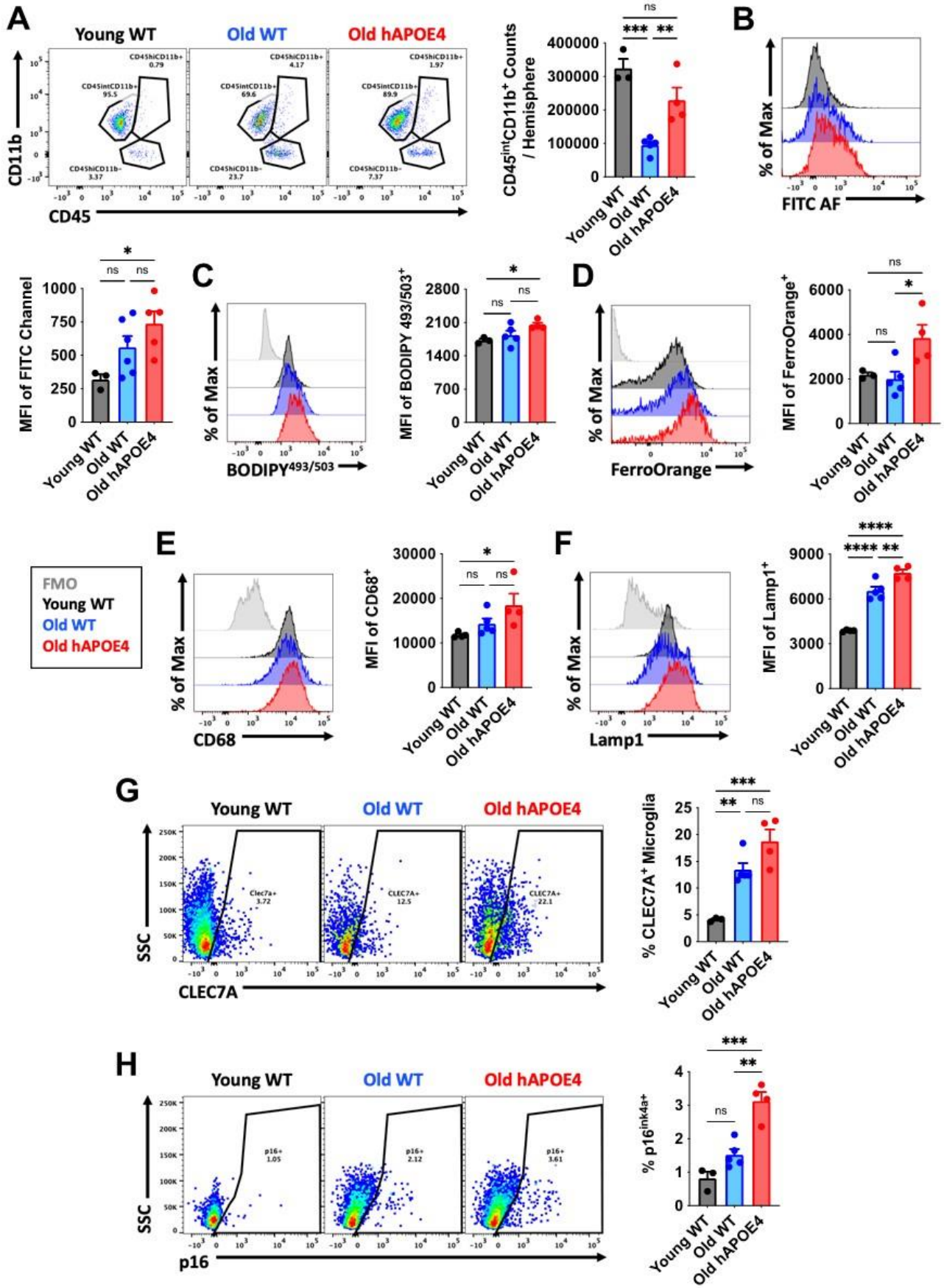

Fig. S7. Age-associated AF phenotype is modified by hAPOE4 genotype.
(A) A representative dot plot illustrates the immune composition in the brain of young and aged C57BL/6, and old, age-matched hAPOE$^{+/+}$ knock-in mice. Microglia from aged hAPOE4 mice displayed significantly higher **(B)** autofluorescence, **(C)** lipid content, **(D)** iron concentration, and expression of **(E)** CD68, **(F)** Lamp1, **(G)** CLEC7a, and **(H)** p16^{ink4a} compared to either young or old wildtype controls. Abbreviations: AF autofluorescence, FMO fluorescence minus one control, max Maximum, MFI mean fluorescence intensity, ns not significant, SSC side scatter, WT wildtype. Data **(A-H)** were analyzed using one-way ANOVA with multiple comparisons (N=3-6/group; *p<0.05, **p<0.01, ***p<0.001, and ****p<0.0001).

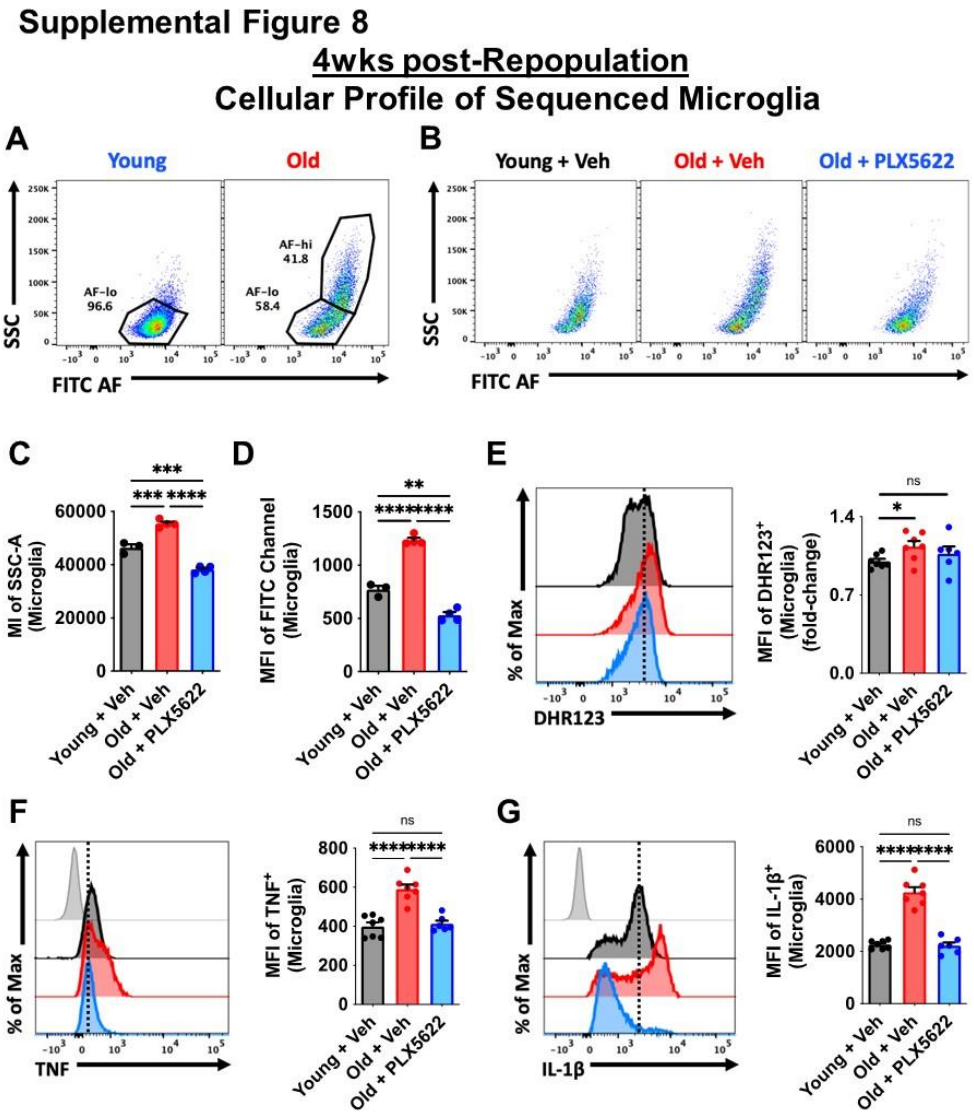

Fig. S8. Cellular profile of microglia sorted for RNA sequencing.
Two sets of experiments were performed to sort microglia for downstream RNA sequencing. In the first, living $CD45^{int}CD11b^{+}Ly6C^{-}$ microglia from young and old wildtype C57Bl/6 male mice were sorted based on the relative level of cellular autofluorescence in the FITC channel **(A)**. FACS sorted microglial subsets (e.g., Old AF^{lo} and Old AF^{hi}) in the first experiment were confirmed autofluorescent based on relative intensity in the FITC channel with respect to the young (i.e., AF^{lo}) group. In the second experiment, rather than sorting by subset, bulk $CD45^{int}Cd11b^{+}Ly6C^{-}$ microglia from young and old vehicle groups and old treatment groups were sorted for comparison **(B)**. Validation of the PLX5622 treatment effect in the bulk sorted groups was performed to show the significant decrease in **(C)** cellular granularity and **(D)** autofluorescence level in microglia following four weeks of repopulation. Microglial production of reactive oxygen species **(E)** and the pro-inflammatory cytokines, TNF **(F)** and IL-1β **(G)** are shown. N=3-4/group **(C-D)** and 6-7/group **(E-G)**. Abbreviations: AF autofluorescent, hi high, lo low, MI mean intensity, MFI mean fluorescence intensity, SSC side scatter, Veh vehicle. Data **(C-G)** were analyzed using one-way ANOVA with multiple comparisons (**p<0.01, ***p<0.001 and ****p<0.0001).

Supplemental Figure 9

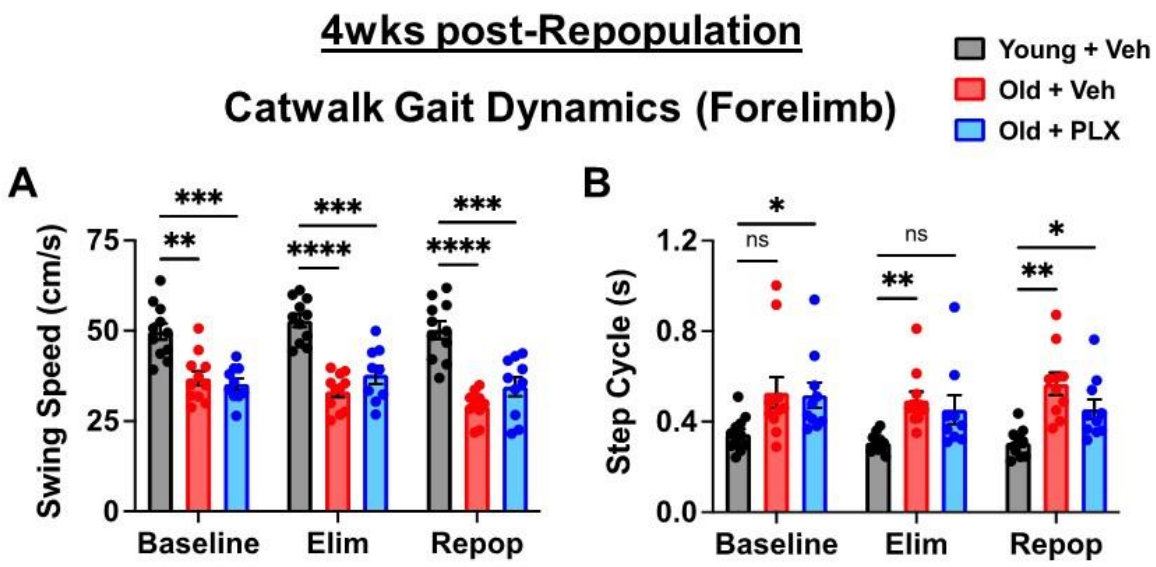

Fig. S9. Assessment of motor function at 4-weeks post-repopulation.
Additional gait measures for forelimb **(A)** swing speed and **(B)** step cycle at four weeks post-repopulation are shown. N=9-11/group. Abbreviations: cm centimeters, Elim elimination phase, ns not significant, PLX PLX5622, Repop repopulation phase, s seconds, Veh vehicle, wks weeks. Data were analyzed using two-way ANOVA with repeated measures (*p<0.05, **p<0.01, ***p<0.001, and ****p<0.0001).

Supplemental Figure 10

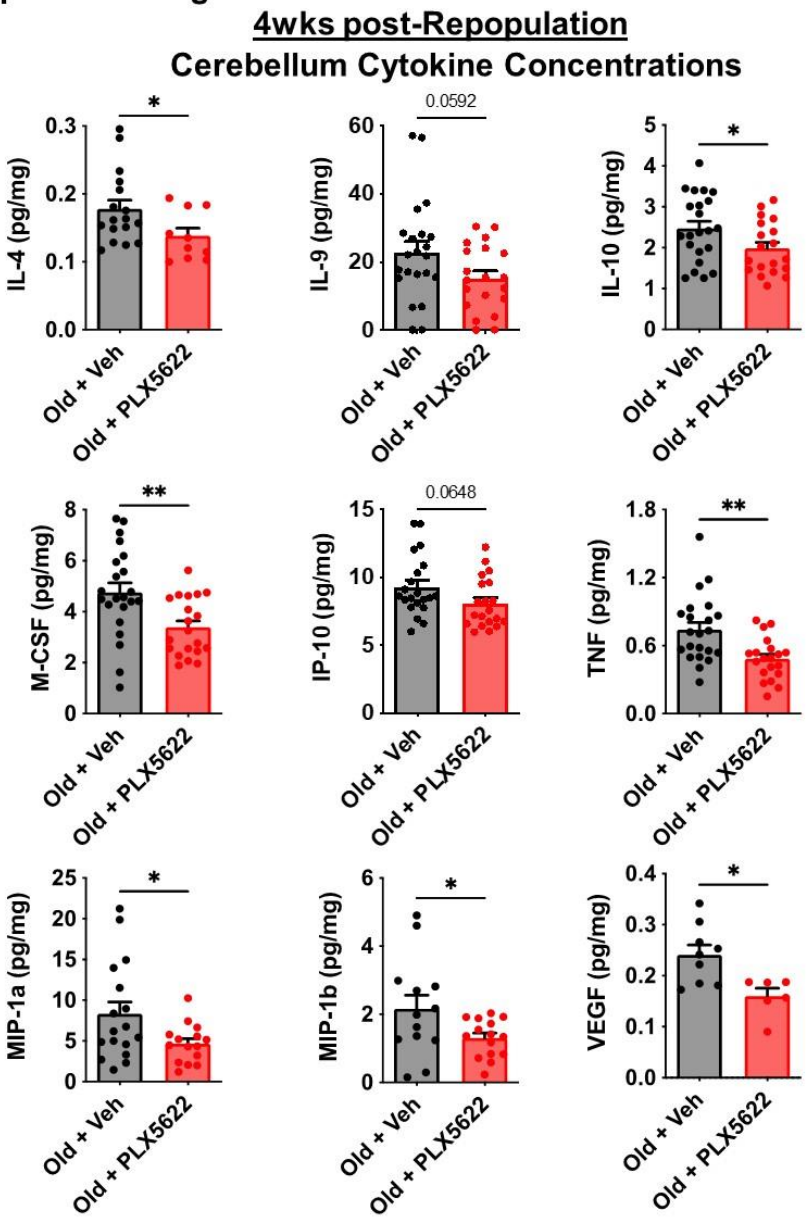

Fig. S10. Cytokine analysis in the aged cerebellum at four weeks after microglial repopulation.

Inflammation in the cerebellum of old mice was examined to better understand the treatment effects on age-related motor function. Out of the 32 analytes tested in a multiplex enzyme-linked immunosorbent assay of inflammatory cytokines, those which were detectable and statistically significant or trending after treatment are shown. Four weeks after microglial repopulation, cerebellar concentrations of IL-4, IL-10, M-CSF, TNF, MIP-1a, MIP-1b, and VEGF were all significantly reduced compared to the vehicle group. Concentrations of IL-9 and IP-10 showed a non-statistical trend for decrease after treatment. N=7-23/group (due to differences in detectability between cytokines). Abbreviations: mg milligram, pg picogram, Veh vehicle. Data were analyzed using Student's t-test (*$p<0.05$ and **$p<0.01$).

Supplemental Figure 11

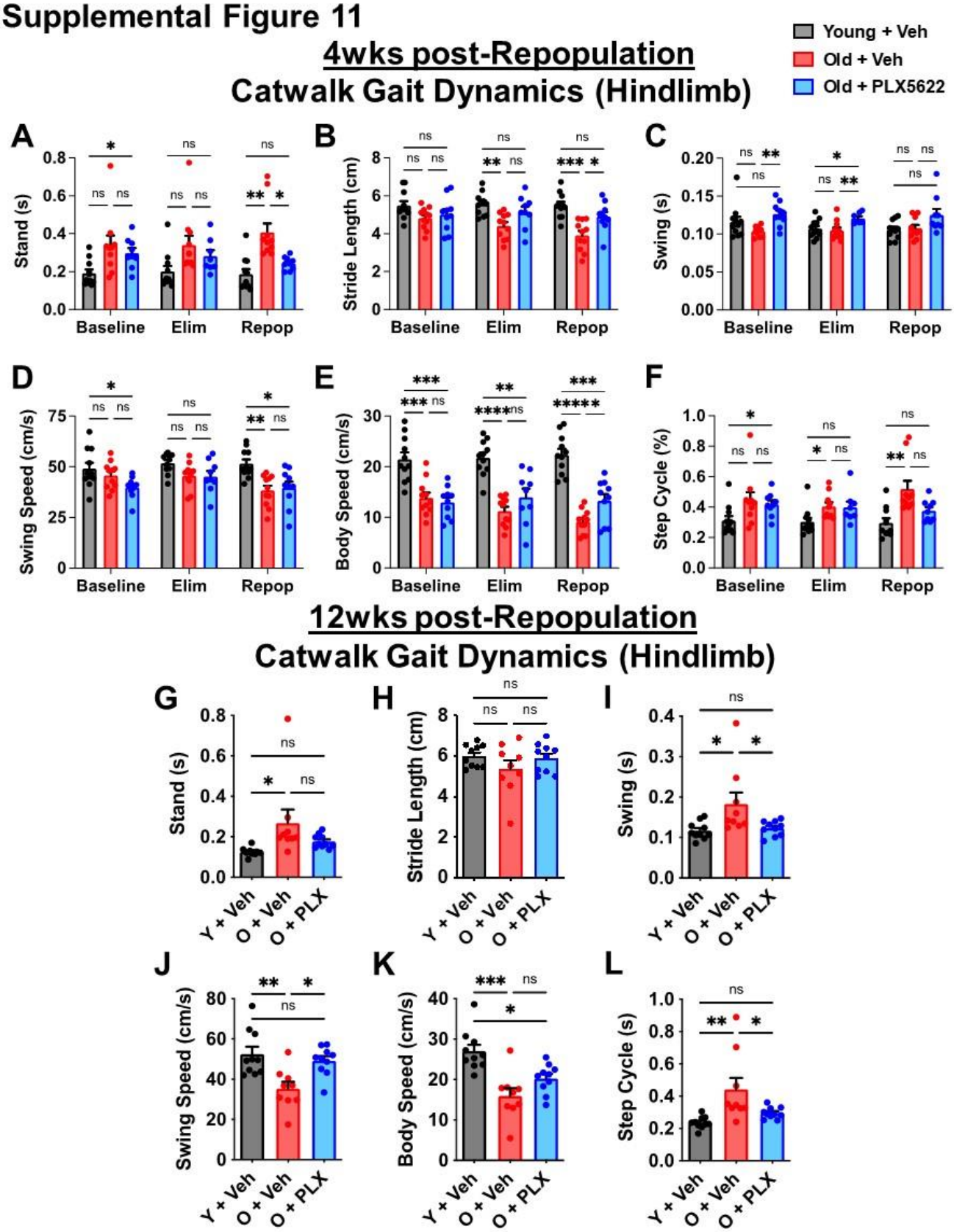

Fig. S11. Assessment of hindlimb gait dynamics at 4- and 12-weeks post-repopulation.
Gait measures for hindlimb (**A**) stand, (**B**) stride length, (**C**) swing, (**D**) swing speed, (**E**) body speed, and (**F**) step cycle at four weeks post-repopulation are shown. At 12 weeks post-repopulation, hindlimb measures for (**G**) stand, (**H**) stride length, (**I**) swing, (**J**) swing speed, (**K**) body speed, and (**L**) step cycle parameters generally mirror that seen in the forelimbs. N=10-11/group **(A-F)**, and 9-10/group **(G-L)**. Abbreviations: cm centimeters, BW body weight, Elim elimination phase, g grams, ns not significant, O old, PLX PLX5622, Repop repopulation phase, s seconds, Veh vehicle, wks weeks, Y young. Data (**A-F**) were analyzed using two-way ANOVA with repeated measures. Data (**G-L**) were analyzed using one-way ANOVA with multiple comparisons (*$p<0.05$, **$p<0.01$, ***$p<0.001$, and ****$p<0.0001$).

Supplemental Figure 12

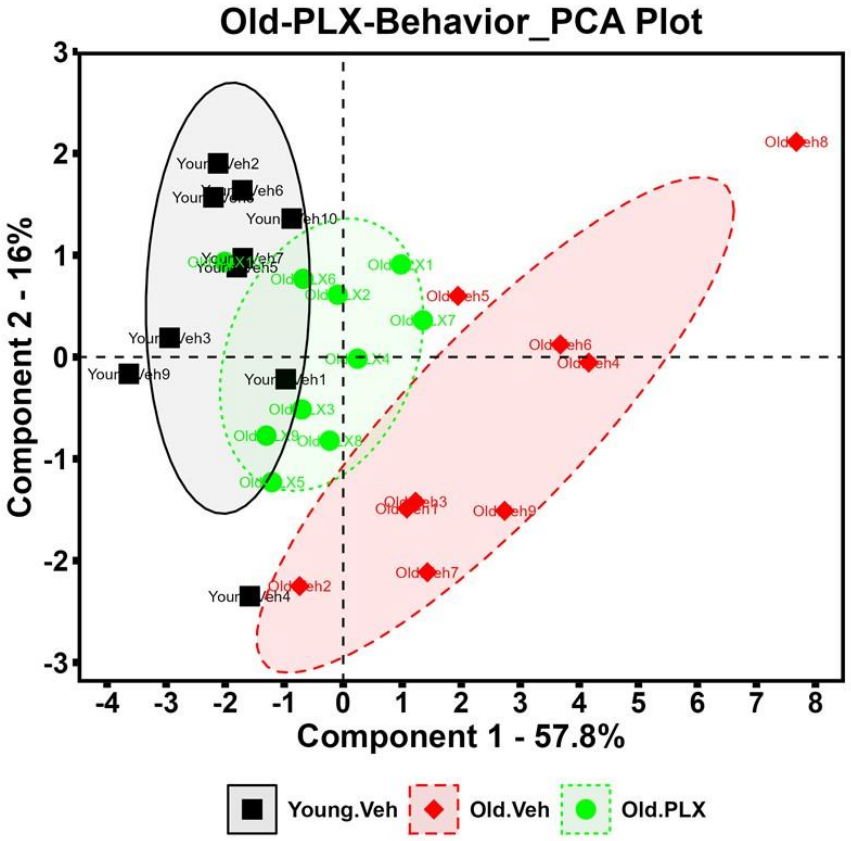

Fig. S12. Principal component analysis of the complete neurobehavioral dataset after 12 weeks post-repopulation.
A principal component analysis (PCA) was generated using the behavioral data presented in **Figure 4J-T**. This integrative data analysis illustrates the partial rejuvenating capacity of forced microglia turnover on affective, cognitive, and motor functions late after repopulation. Abbreviations: Veh vehicle.

Supplemental Figure 13

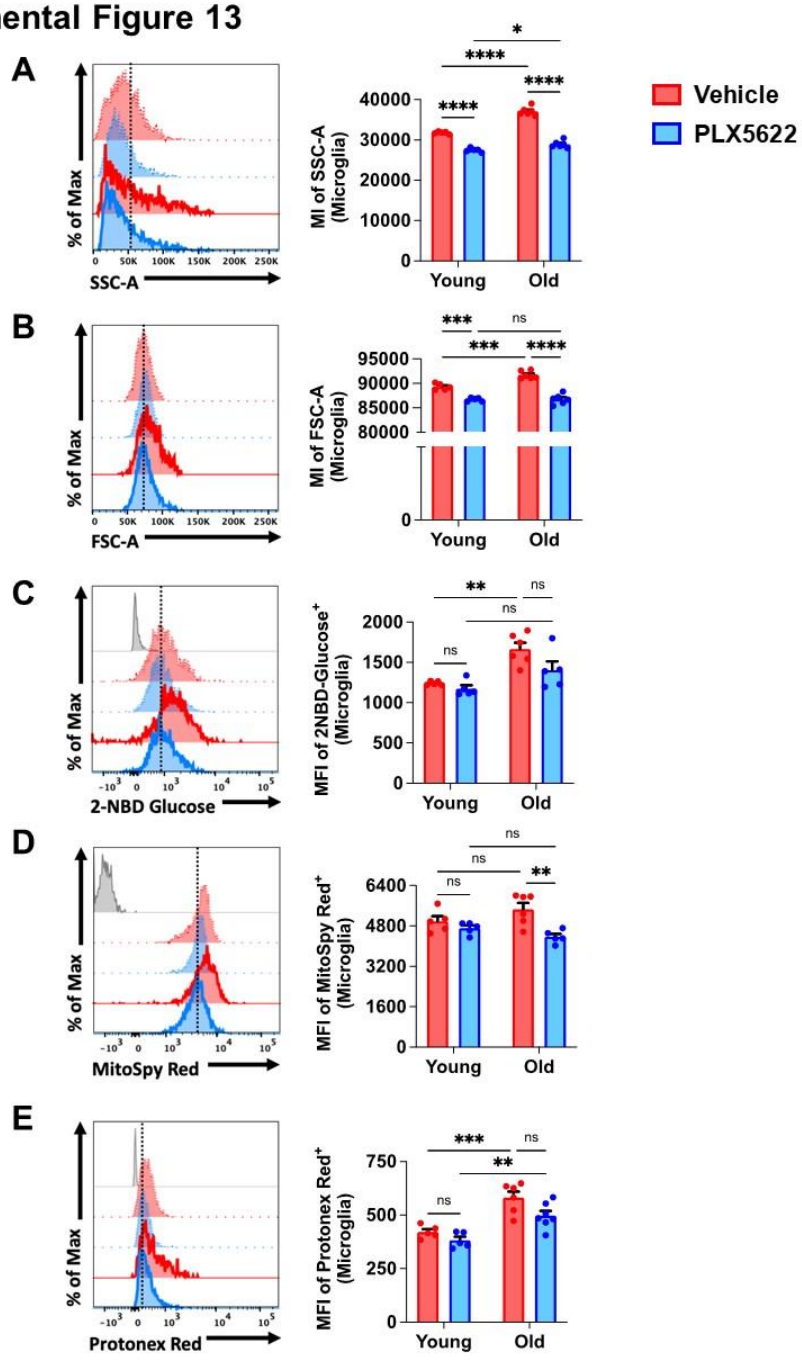

Fig. S13. Assessment of microglia phenotype at 12 weeks post-repopulation.
Repopulated microglia from old mice treated with PLX5622 displayed significant reductions in **(A)** cell granularity, **(B)** cell volume, **(C)** glucose uptake, **(D)** mitochondrial membrane potential, and **(E)** cytosolic acidosis as evidenced by MFI quantification of the representative histograms. N=4-6/group. Abbreviations: FSC forward scatter, Max maximum, MFI mean fluorescence intensity, ns not significant, SSC side scatter. Data **(A-E)** were analyzed using two-way ANOVA group analysis with multiple comparison's test (*p<0.05, **p<0.01, ***p<0.001, and ****p<0.0001).

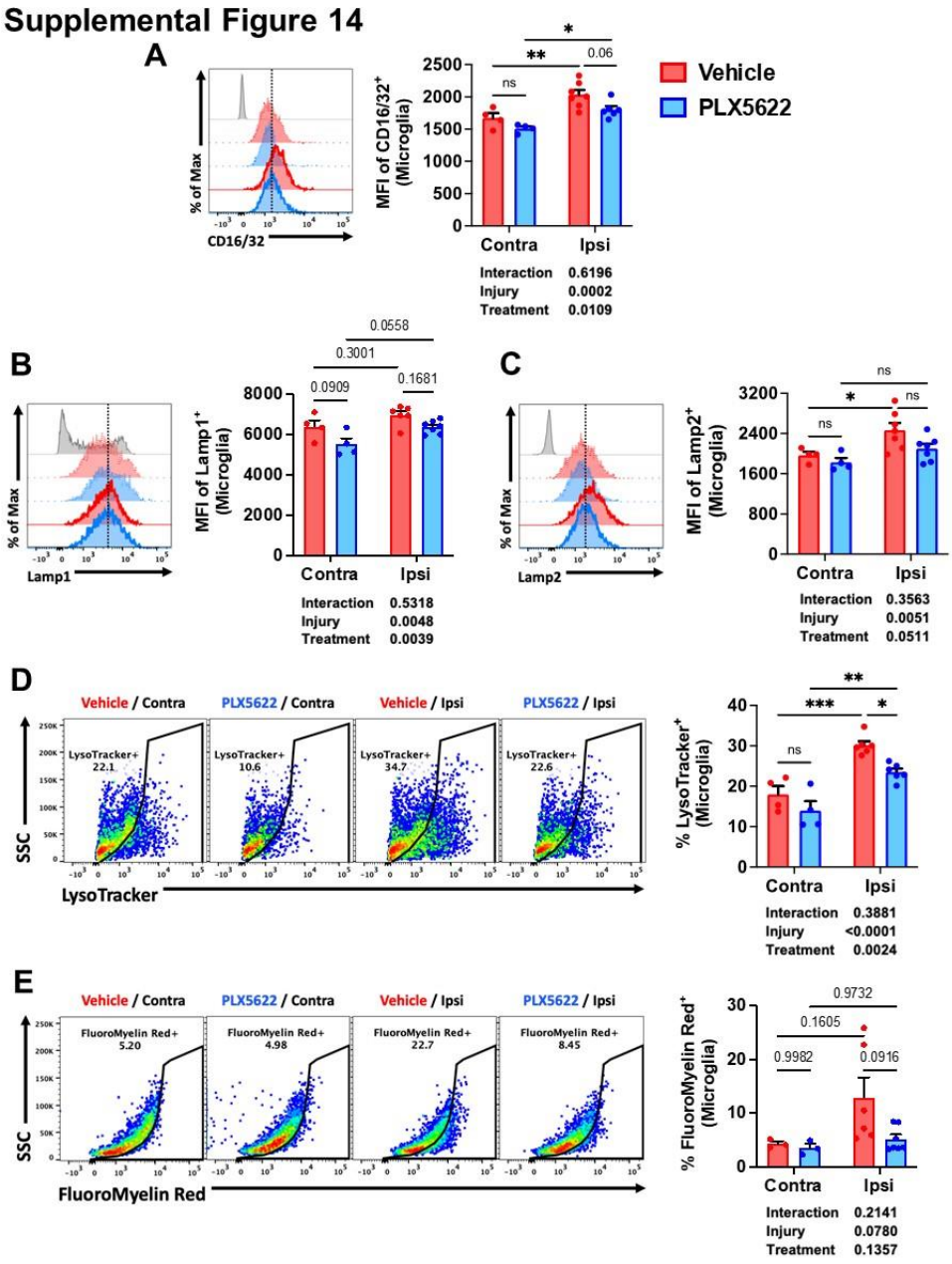

Fig. S14. Effect of repopulation on microglial phenotype at two weeks post-TBI.
Old mice were treated with vehicle or PLX5622 for two weeks, followed by 12 weeks of repopulation prior to TBI. Microglia in the injured ipsilateral and contralateral control hemisphere were evaluated for phagocytosis and autophagy markers at 2 weeks post-TBI. Representative histograms and relative MFI quantification show that repopulated microglia exhibit treatment effects in **(A)** CD16/32, **(B)** Lamp1, and **(C)** Lamp2 expression compared to the vehicle group after injury. Representative dot plots also demonstrate significant TBI-related reductions in the frequency of **(D)** LysoTracker-positive and **(E)** Fluoromyelin Red-positive microglia. Abbreviations: Contra contralateral, Ipsi ipsilateral, max Maximum, MFI mean fluorescence intensity, ns not significant, SSC side scatter. Data **(A-E)** were analyzed using two-way ANOVA with multiple comparisons (N=4-7/group; *p<0.05, **p<0.01, and ***p<0.001).

Supplemental Figure 15

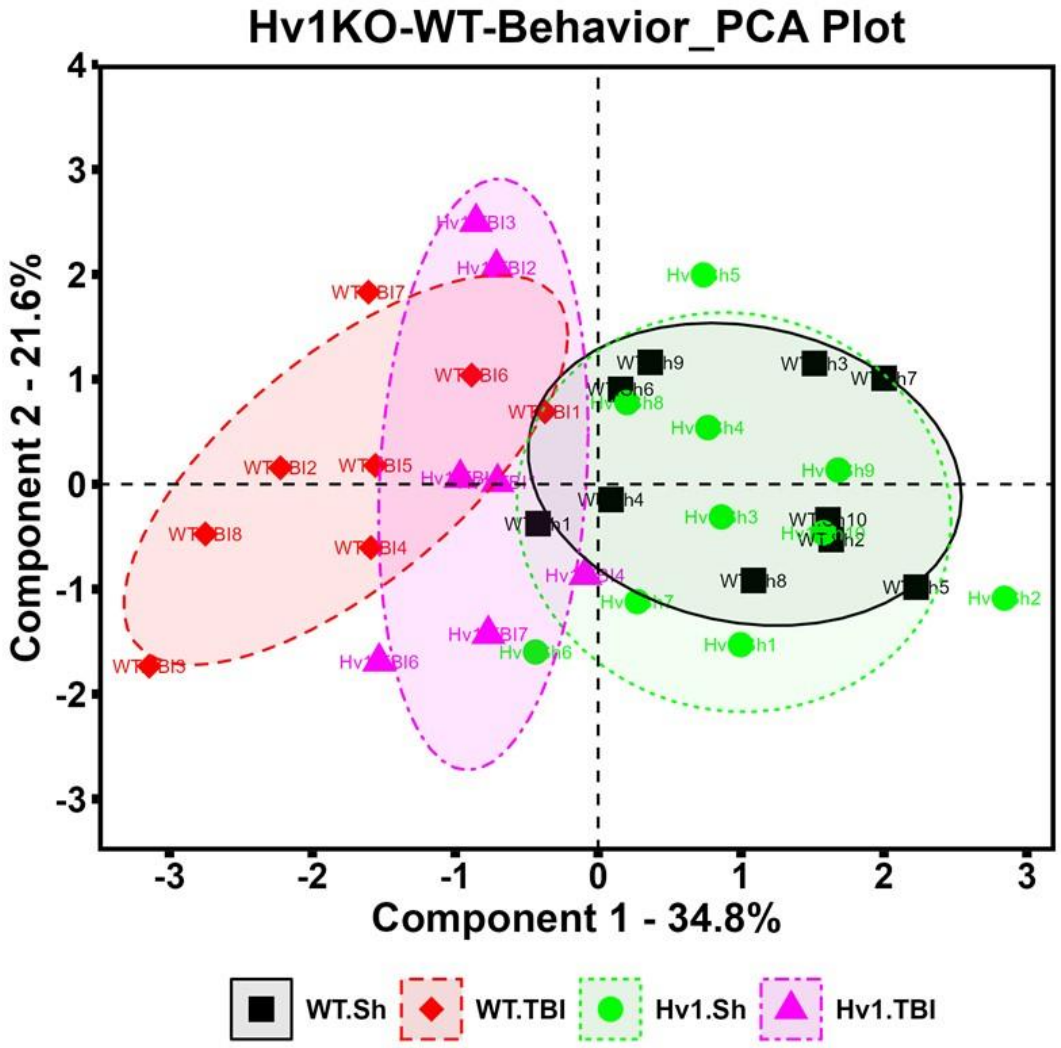

Fig. S15. Principal component analysis of the complete neurobehavioral dataset at one-year post-TBI in WT and Hv1-knockout mice.

A principal component analysis (PCA) was generated using the behavioral data presented in **Figure 10E-J**. This integrative data analysis illustrates more simply the attenuating effects of Hv1-knockout on long-term neurological deficits in affective, cognitive, and motor functions late after TBI. Abbreviations: WT wildtype, KO knockout, Sh sham, TBI traumatic brain injury, Hv1 Voltage-gated hydrogen channel 1.

Supplemental Figure 16

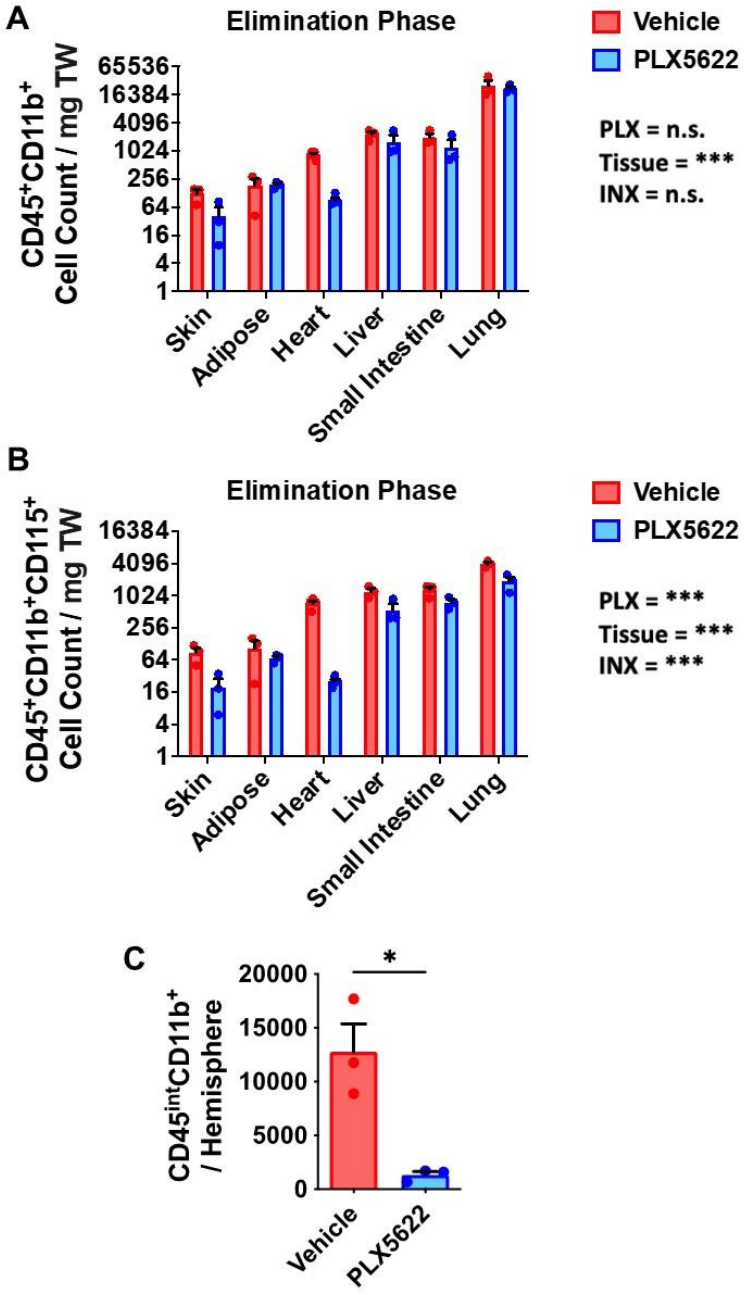

Fig. S16. Peripheral immune composition following short-term CSF1R inhibition with PLX5622.

(A) Cell counts of $CD45^{+}CD11b^{+}$ immune cells in multiple organs was quantified using flow cytometry at two-weeks after continuous treatment with PLX5622 in young male mice. **(B)** Further refinement of the gating strategy to include $CD115^{+}$ cells, which express CSF1R, show even higher significance as evidenced by two-way ANOVA group interaction. **(C)** The number of brain microglia was significantly reduced during PLX5622 treatment. N=3-5/group. Abbreviations: INX interaction, mg milligrams, PLX Plexxikon 5622, TW tissue weight. Data **(A-B)** were analyzed using two-way ANOVA with Bonferroni's post-hoc correction. Data **(C)** were analyzed using Student's t-test (*$p<0.01$ and ***$p<0.001$).

Supplemental Table 1 - Genes related to pathway analysis (Figure 3)

https://www.gsea-msigdb.org/gsea/msigdb/human/geneset/GOBP_PHAGOCYTOSIS

GOBP_PHAGOCYTOSIS (M16307)						
ABCA1	CDC42	ICAM3	IGHV4-28	MARCO	PTPRJ	TICAM2
ABCA7	CDC42SE1	ICAM5	IGHV4-31	MBL2	PTX3	TIMD4
ABL1	CDC42SE2	IFNG	IGHV4-34	MEGF10	PYCARD	TLR2
ADGRB1	CEACAM4	IGHA1	IGHV4-39	MERTK	RAB11FIP2	TLR4
ADIPOQ	CEBPE	IGHA2	IGHV4-4	MESD	RAB14	TM9SF4
ADORA1	CFP	IGHD	IGHV4-59	MET	RAB20	TMEM175
ADORA2A	CLCN3	IGHE	IGHV4-61	MFGE8	RAB27A	TNF
AHSG	CLEC7A	IGHG1	IGHV5-10-1	MIR17	RAB31	TRBC1
AIF1	CLN3	IGHG2	IGHV5-51	MIR181B1	RAB34	TRBC2
ALOX15	CNN2	IGHG3	IGHV6-1	MIR183	RAB39A	TRDC
ANO6	COLEC10	IGHG4	IGHV7-4-1	MIR20A	RAB5A	TREM2
ANXA1	COLEC11	IGHM	IGHV7-81	MSR1	RAB7A	TREX1
ANXA11	COLEC12	IGHV1-18	IGKC	MST1R	RAB7B	TUB
ANXA3	CORO1A	IGHV1-24	IGLC1	MYD88	RAC1	TULP1
APOA1	CORO1C	IGHV1-3	IGLC2	MYH9	RAC2	TUSC2
APOA2	CRP	IGHV1-45	IGLC3	MYO18A	RACK1	TYRO3
APPL1	CRYBA1	IGHV1-58	IGLC6	MYO1G	RARA	TYROBP
APPL2	CSK	IGHV1-69	IGLC7	MYO7A	RHOBTB1	UNC13D
ARHGAP12	CYBA	IGHV1-69-2	IGLL1	NCF2	RHOBTB2	VAMP7
ARHGAP25	DNM2	IGHV1-69D	IGLL5	NCF4	RHOG	VAV1
ARL8B	DOCK1	IGHV2-26	IL15	NCKAP1L	RHOH	VAV2
ATG3	DOCK2	IGHV2-5	IL15RA	NOD2	RUBCN	VAV3
ATG5	DYSF	IGHV2-70	IL1B	OLFM4	SCARB1	VIPAS39
AXL	EIF2AK1	IGHV2-70D	IL2RB	P2RX7	SFTPA1	VPS33B
AZU1	ELANE	IGHV3-11	IL2RG	P2RY6	SFTPD	XKR4
BCR	ELMO1	IGHV3-13	IRF8	PAK1	SH3BP1	XKR5
BECN1	ELMO2	IGHV3-15	ITGA2	PEAR1	SIRPA	XKR6
BIN2	ELMO3	IGHV3-16	ITGAL	PECAM1	SIRPB1	XKR7
BTK	F2RL1	IGHV3-20	ITGAM	PIK3CA	SIRPG	XKR8
C1orf43	FCER1G	IGHV3-21	ITGAV	PIKFYVE	SLAMF1	XKR9
C2	FCGR1A	IGHV3-23	ITGB1	PIP4P2	SLC11A1	YES1
C3	FCGR2B	IGHV3-30	ITGB2	PIP5K1A	SNX3	
C4A	FCN1	IGHV3-33	ITGB3	PIP5K1C	SOD1	
C4B	FCN2	IGHV3-35	JMJD6	PLA2G5	SPACA3	
C4BPA	FCN3	IGHV3-38	KIAA1109	PLA2G6	SPG11	
C4BPB	FER1L5	IGHV3-43	LBP	PLCG2	SPHK1	
CALR	FGR	IGHV3-48	LDLR	PLD2	SPON2	
CAMK1D	FPR2	IGHV3-49	LEP	PLD4	SRC	
CCL2	FYN	IGHV3-53	LEPR	PLPP4	SRPX	
CD14	GAS6	IGHV3-64	LETMD1	PLSCR1	STAP1	
CD300A	GATA2	IGHV3-64D	LIMK1	PRKCD	SYK	
CD300LF	GSN	IGHV3-66	LMAN2	PRKCE	SYT11	
CD302	GULP1	IGHV3-7	LRP1	PRKCG	SYT7	
CD36	HAVCR1	IGHV3-72	LYAR	PRTN3	TAFA4	
CD47	HCK	IGHV3-73	LYN	PTK2	TGM2	
CD93	HMGB1	IGHV3-74	LYST	PTPRC	THBS1	

https://www.gsea-msigdb.org/gsea/msigdb/human/geneset/GOBP_REGULATION_OF_AUTOPHAGY

GOBP_REGULATION_OF_AUTOPHAGY (M10281)						
ABL1	CAMKK2	EXOC1	KAT5	NPRL3	RNF5	TBC1D25
ABL2	CAPN1	EXOC4	KAT8	NRBP2	ROCK1	TBK1
ACER2	CAPNS1	EXOC7	KAT8	NUPR1	RPTOR	TECPR1
ADRA1A	CASP3	EXOC8	KDM4A	OPTN	RRAGA	TFEB
ADRB2	CCNY	FBXL2	KDR	ORMDL3	RRAGB	TICAM1
AKT1	CDK16	FBXO7	KEAP1	OSBPL7	RRAGC	TIGAR
AMBRA1	CDK5	FBXW7	KIF25	PAFAH1B2	RRAGD	TLK2
ATF6	CDK5R1	FEZ1	KLHL22	PARK7	RUBCN	TLR9
ATG101	CERS1	FEZ2	LACRT	PARL	RUFY4	TMEM39A
ATG12	CHMP4A	FLCN	LAMP3	PHF23	SCFD1	TMEM59
ATG13	CHMP4B	FOXK1	LARP1	PIK3C2A	SCOC	TOM1
ATG14	CISD1	FOXK2	LEP	PIK3C3	SEC22B	TP53
ATG16L1	CISD2	FOXO1	LEPR	PIK3CA	SESN1	TP53INP1
ATG2A	CLEC16A	FOXO3	LRRK2	PIK3CB	SESN2	TP53INP2
ATG5	CLN3	FYCO1	LRSAM1	PIK3R2	SESN3	TPCN1
ATM	CPTP	FZD5	LZTS1	PIK3R4	SH3BP4	TPCN2
ATP13A2	CRYBA1	GAPDH	MAGEA3	PIM2	SH3GLB1	TREM2
ATP6V0A1	CSNK2A2	GATA4	MAGEA6	PINK1	SIRT1	TRIB3
ATP6V0A2	CTSA	GBA	MAP3K7	PIP4K2A	SIRT2	TRIM13
ATP6V0B	CTTN	GFAP	MAPK15	PIP4K2B	SLC25A4	TRIM14
ATP6V0C	DAP	GNAI3	MAPK3	PIP4K2C	SLC25A5	TRIM21
ATP6V0D1	DAPK1	GOLGA2	MAPK8	PLEKHF1	SLC7A5	TRIM22
ATP6V0D2	DAPK2	GPR137	MAPT	PLK2	SMCR8	TRIM27
ATP6V0E1	DAPK3	GPR137B	MCL1	PLK3	SMG1	TRIM32
ATP6V0E2	DAPL1	GPSM1	MEFV	POLDIP2	SNCA	TRIM34
ATP6V1A	DCAF12	GSK3A	MET	PRKAA1	SNRNP70	TRIM38
ATP6V1B1	DCN	GSK3B	MFSD8	PRKAA2	SNX18	TRIM5
ATP6V1B2	DDIT3	HAX1	MID2	PRKACA	SNX30	
ATP6V1C1	DEPDC5	HDAC6	MIR199A1	PRKD1	SNX32	
ATP6V1C2	DEPP1	HERC1	MIRLET7B	PRKN	SNX4	
ATP6V1D	DHRSX	HGF	MLST8	PSAP	SNX5	
ATP6V1E1	DNM1L	HIF1A	MOAP1	PTPN22	SNX6	
ATP6V1E2	DRAM1	HMGB1	MT3	PYCARD	SNX7	
ATP6V1G1	DRAM2	HMOX1	MTCL1	QSOX1	SOGA1	
ATP6V1G2	EEF1A1	HSPB1	MTDH	RAB39B	SOGA3	
ATP6V1H	EEF1A2	HSPB8	MTM1	RAB3GAP1	SPTLC1	
BAD	EHMT2	HTR2B	MTMR3	RAB3GAP2	SPTLC2	
BAG3	EIF4E	HTRA2	MTMR4	RAB8A	SREBF1	
BCL2	EIF4G1	HTT	MTMR8	RALB	SREBF2	
BCL2L11	EIF4G2	IFI16	MTMR9	RASIP1	STAT3	
BECN1	EIF4G3	IFNG	MTOR	RB1CC1	STING1	
BMF	ELAPOR1	IKBKG	NEDD4	RHEB	STK11	
BNIP3	ENDOG	IL10	NLRP6	RIPK2	SUPT5H	
BNIP3L	EP300	IL10RA	NOD1	RMC1	SVIP	
BOK	EPM2A	IL4	NOD2	RNF152	TAB2	
C9orf72	ERCC4	IRGM	NPC1	RNF31	TAB3	
CALCOCO2	ERN1	ITPR1	NPRL2	RNF41	TBC1D14	

https://www.gsea-msigdb.org/gsea/msigdb/human/geneset/GOBP_REGULATION_OF_REACTIVE_OXYGEN_SPECIES_BIOSYNTHETIC_PROCESS

GOBP REGULATION OF REACTIVE OXYGEN SPECIES BIOSYNTHETIC PROCESS (M15379)						
ABCB7	CD36	DUOXA2	MIR21	MTCO2P12	RAB27A	SOD2
ABCD1	CFLAR	FOXO3	MIR24-1	NDUFC2	RHOA	SPHK2
ABCD2	CLCN3	FYN	MIR590	PAGE4	SLC18A2	TLR4
ADGRB1	COA8	GRIN1	MIR675	PARK7	SLC25A33	TLR6
ALOX5	CTNS	H19	MMP8	PIKFYVE	SLC30A10	TRAP1
ARG2	CYBA	INS	MPV17L	PLCG2	SLC5A3	UCP1
CCN6	DUOXA1	MIR181A2	MT-CO2	PPARA	SNCA	ZNF205

[(*1*) Y. Hu, et al., Cell Rep. 2021 Jun 8;35(10):109228. doi: 10.1016/j.celrep.2021.109228.]

DAM/SENESCENCE						
Cst7	Lpl	Spp1	Itgax	Cdkn1a	Casp8	Glb1
Csf1	Apoe	Cd74	Cdkn2a	Cdkn2d	Il1b	Serpine1